NASA TECHNICAL MEMORANDUM

NASA TM X-68051

NASA TM X-68051

COMPARISON OF EXPERIMENTAL AND THEORETICAL THERMAL FATIGUE LIVES FOR FIVE NICKEL-BASE ALLOYS

by David A. Spera
Lewis Research Center
Cleveland, Ohio

TECHNICAL PAPER proposed for presentation at Symposium on Fatigue at Elevated Temperatures sponsored by the American Society for Testing and Materials
Starrs, Connecticut, June 18-23, 1972

COMPARISON OF EXPERIMENTAL AND THEORETICAL THERMAL FATIGUE LIVES FOR FIVE NICKEL-BASE ALLOYS

by David A. Spera

Lewis Research Center
Cleveland, Ohio

E-6852

ABSTRACT

Alloys investigated were Nimonic 90, IN 100, coated IN 100, B 1900, coated B 1900, MAR M200, and MAR M200DS (directionally solidified). Maximum temperatures ranged from 770 C to 1120 C (1420 F to 2050 F). Specimen geometries included tapered disks, double-edged wedges, and cambered airfoils. The disks and wedges were heated and cooled in fluidized beds. The airfoil specimens were heated by a Mach 1 natural gas burner and rapid-air cooled, with and without spanwise loading. Life calculations included two distinct failure modes: conventional low-cycle fatigue and cyclic creep. Required material properties were limited to conventional thermal, tensile, and creep-rupture data. The complete life calculation system included the calculation of transient temperature distributions, thermal strains, stresses, creep damage, fatigue damage, and finally cycles to first crack. Calculated lives were within a factor of two for 76 of the 86 data points analyzed. Cyclic creep accounted for 81% of all the calculated damage.

INTRODUCTION

The purpose of this investigation is to evaluate a theory for calculating thermal fatigue life. This theory has evolved from previous work at the Lewis Research Center (ref. 1 to 3) and from earlier work by Robinson (ref. 4) and Taira (ref. 5). All indications are that this evolutionary process will continue. For example, integration of the new concept of "strain-range

partitioning'' (ref. 6) is now being investigated.

The complete life calculation system contains many simplifying assumptions concerning details of heat transfer, thermal stress analysis, plasticity, creep, cumulative damage, crack initiation, etc. Space limitations prohibit examining these assumptions in detail here. However, they will be discussed thoroughly in a forthcoming NASA publication.

Test data were obtained from three sources: the National Gas Turbine Establishment (ref. 7) for Nimonic 90 tapered-disk data; the IIT Research Institute (refs. 8 and 9) for IN 100, B 1900, MAR M200, and MAR M200DS double-wedge data; and the Lewis Research Center (ref. 10) for IN 100 and B 1900 cambered-airfoil data. Mechanical properties required for analysis were always limited to conventional tensile and creep-rupture data for the alloy in its as-received condition.

STRAIN-TEMPERATURE-TIME CALIBRATION

Life analysis starts with the calculation of temperature and mechanical strain cycles at possible points of failure. These calculations are made for representative values of the primary variable which may be maximum temperature, cycle time, or external load. This forms a strain-temperature-time calibration curve from which to extrapolate to other values of the primary variable. Thermocouple data and a thermoelastic strain analysis are the basis of this calibration. For the airfoil specimens, data from infra-red photographs, an electro-optical pyrometer, and an electro-optical extensometer were also used.

Figure 1 shows typical strain-temperature-time calibration curves for the three geometries analyzed, for representative alloys. Wide variations among these curves are apparent. Since time, temperature, and strain interact to produce failure, an analytical method becomes essential in correlating various laboratory tests and actual service.

ELASTIC-PLASTIC-CREEP STRESS ANALYSIS

The elastically-computed mechanical strains were assumed to remain constant in the presence of local plastic flow and creep, as proposed in refer-

ence 11. The mechanical strain cycle was divided into small increments in order to compute its elastic, plastic, and creep components. Successive iteration was required to produce a stable, repeating hysteresis loop. Details of the cyclic thermal stress analysis will be given in a forthcoming NASA publication. In general, it is a complex but necessary part of the complete life calculation system.

LIFE CALCULATION THEORY

The life calculation theory used in this study is described in reference 3. This theory states that thermal fatigue is a combination of conventional low-cycle fatigue and cyclic creep rupture. Low-cycle fatigue is assumed to be time-independent and usually results in failure by transgranular cracking. On the other hand, cyclic creep rupture is assumed to be time-dependent and usually causes intergranular cracking. Life is calculated separately for each of these two distinct failure modes. A linear interaction between fatigue and cyclic creep lives is assumed. This assumption is made primarily for convenience, since one mode is usually dominant. Thermal fatigue life can then be calculated as follows:

$$\frac{1}{N_t} = \frac{1}{N_c} + \frac{1}{N_f} \tag{1a}$$

or

$$N_t = (\varphi_c + \varphi_f)^{-1} \tag{1b}$$

in which

N cycles to failure

φ damage per cycle, 1/N

t, c, f thermal fatigue, cyclic creep, and low cycle fatigue, respectively

In this investigation, approximately 80% of all the calculated damage was by cyclic creep, with 20% by fatigue.

Cyclic Creep Damage

Cyclic creep damage, φ_c, is calculated from conventional creep-rupture data. A modification of the life-fraction rules proposed by Robinson and Taira (refs. 4 and 5) is used, as follows:

$$\varphi_c = \int_0^{\Delta t} \frac{dt}{k t_r(|S|, T)} \tag{2}$$

in which

t elapsed time, hr

Δt time per cycle, hr

t_r conventional creep rupture life, hr

$|S|$ absolute value of instantaneous stress, N/cm^2

T instantaneous temperature, ^oC

k 1, for uncoated alloys; or D/D' for coated alloys assuming cracks initiate in the substrate

in which

D tensile ductility at temperature T, cm/cm

D' average creep strain during first and second stages at temperature T, cm/cm

The two values of k are derived from the idealized creep-rupture behavior shown in figure 2. First and second stages of creep are linearized, with a constant creep rate $\dot{\epsilon}_c$. Unstable third-stage creep occurs at a strain of D' and a time t_r, the conventional creep-rupture life. However, if the creep rate were held constant, it is assumed that rupture would not occur until the creep strain equals the ductility D. Thus the "stable" rupture time would be longer than the "unstable" or conventional rupture life by a factor of D/D'. This is similar to behavior proposed in reference 12.

Cyclic creep-rupture is also assumed to occur in either a stable or unstable mode. Isothermal strain cycling, balanced in tension and compression, is usually stable, as discussed in reference 12. However, thermal

fatigue cycles are potentially unstable. Creep strains in tension and compression are rarely in balance. Usually creep occurs in only one half-cycle and is balanced by time-independent plasticity in the other. Two different flow mechanisms are usually present, with creep occurring at the grain boundaries and plasticity within grains. On an uncoated surface, accumulation of creep at a grain boundary or other discontinuity can cause local bulging or necking. This is assumed to be unstable deformation analogous to conventional creep rupture, and k is therefore taken equal to 1.

Grain size can be expected to influence the distribution of inelastic strain along the surface of the material. A fine-grained structure should produce a more uniform distribution of tensile and compressive inelastic strain. Following this hypothesis, it is assumed that a fine-grained, oxidation-resistant coating distributes inelastic strain uniformly along the surface of the substrate, preventing local deformation at grain boundaries. For a coated alloy, then, deformation is assumed to be stable and k is taken equal to D/D'.

The assumption that cracks initiate in the substrate is consistent with the qualities of good high-temperature coatings: oxidation resistance, reasonable ductility, metallurgical bonding, compatible thermal expansion, etc.

Low-Cycle Fatigue Damage

Fatigue damage φ_f was calculated by Manson's Method of Universal Slopes (ref. 11). This is an empirical formula relating mechanical strain range, cycles to failure (or fatigue damage), and conventional tensile properties, as follows:

$$\varphi_f = \frac{1}{N_f}, \text{ fatigue damage}$$

$$\Delta\epsilon_m = 3.5 \frac{UTS}{E} \varphi_f^{.12} + D^{.6} \varphi_f^{.6} \tag{3}$$

$\Delta\epsilon_m$ mechanical strain range, cm/cm

UTS ultimate tensile strength, N/cm^2

E Young's Modulus, N/cm^2

D tensile ductility, cm/cm

Equation (3) can be solved either graphically or numerically for φ_f. To be conservative, tensile properties were evaluated at the temperature in the cycle which gives the minimum life (maximum φ_f). This is usually the maximum temperature in the cycle.

The Method of Universal Slopes has been used successfully to correlate data for a wide variety of alloys. However, for a specific alloy, some other empirical formula or fatigue data could be substituted if available.

RESULTS

Figures 3 to 8 present comparisons between observed and calculated thermal fatigue lives for the various alloys and test conditions. Lives are given as "cycles to first crack" which was determined in one of two ways: In the fluidized-bed tests, it was the average of the last inspection cycle without cracks and the first inspection cycle with cracks. In the burner-rig tests, sufficient crack propagation data were obtained to extrapolate backwards to "zero" crack length, and that cycle was taken as the life.

In figure 3, representative fatigue and cyclic creep lives are shown for tapered-disk specimens, together with their linear interaction. In figures 4, 5, and 6 data for the two different edge radii on double-wedge specimens are compared with the curves for the 0.6 millimeter radius edge. For convenience, the data for the 1.0 millimeter radius edges have been scaled to 0.6 mm, maintaining the same ratio of calculated to observed life (ref. 9).

Life calculations for MAR M200DS (fig. 6) included a first-order correction for sharpening of the edge radius through erosion of the wedge surfaces. Erosion was found to be relatively high in this directional alloy (ref. 9). This correction produced a 15% reduction in calculated life for the 6 minute cycle. Erosion corrections for the other alloys were negligible.

For the airfoil tests (figs. 7 and 8), it was necessary to include the effect of the Mach 1 gas velocity on the static creep-rupture time t_r in equation (2). As discussed in reference 10, this high gas velocity can cause

losses in life amounting to more than 90% at 1000° C.

CONCLUDING REMARKS

Calculated lives were within a factor of two for 76 of the 86 data points analyzed. Log standard deviation was 0.2, or a factor of 1.6. Cyclic creep accounted for 81% of all the calculated damage. Further evaluation is recommended, particularly using data on cobalt- and iron-base alloys and specimens with stress concentrations and vibration.

REFERENCES

1. Manson, S. S., International Journal of Fracture Mechanics, IJFM-A, Vol. 2, No. 1, March 1966, pp. 327-363.

2. Spera, D. A., "A Linear Creep Damage Theory for Thermal Fatigue of Materials," Ph. D. Thesis, University of Wisconsin, Madison, 1968.

3. Spera, D. A., "The Calculation of Elevated Temperature Cyclic Life Considering Low-Cycle Fatigue and Creep," NASA TN D-5317, National Aeronautics and Space Administration, July 1969.

4. Robinson, E. L., "Effect of Temperature Variation on the Long-Time Rupture Strength of Steels," Transactions ASME, TASMA, Vol. 74, No. 5, July 1952, pp. 777-781.

5. Taira, S., Creep in Structures, N. J. Hoff, ed., Springer-Verlag, Berlin, 1962, pp. 96-124.

6. Halford, G. R., Hirschberg, M. H., and Manson, S. S., "Temperature Effects on the Strainrange Partitioning Approach for Creep-Fatigue Analysis," NASA TM X-68023, National Aeronautics and Space Administration, June 1972.

7. Glenny, E. and Taylor, T. A., Journal of the Institute of Metals, JIME-A, Vol. 88, 1959-1960, pp. 449-461.

8. Howes, M. A. H., "Thermal Fatigue Data on 15 Nickel- and Cobalt-Base Alloys," IITRI-B6078-38, Illinois Institute of Technology Research Institute, Chicago, Illinois, 1970.

9. Spera, D. A., Howes, M. A. H., and Bizon, P. T., "Thermal-Fatigue Resistance of 15 High-Temperature Alloys Determined by the Fluidized-Bed Technique," NASA TM X-52975, National Aeronautics and Space Administration, March 1971.

10. Spera, D. A., Calfo, F. D., and Bizon, P. T., "Thermal Fatigue Testing of Simulated Turbine Blades," NASA TM X-67820, National Aeronautics and Space Administration, May 1971.

11. Manson, S. S., "Fatigue: A Complex Subject - Some Simple Approximations," Experimental Mechanics, EXMC-A, Vol. 5, No. 7, July 1965, pp. 193-226.

12. Swindeman, R. W., "The Interrelation of Cyclic and Monotonic Creep Rupture," Proceedings of the Joint International Conference on Creep, Institution of Mechanical Engineers, London, 1963, pp. 3-71 to 3-76.

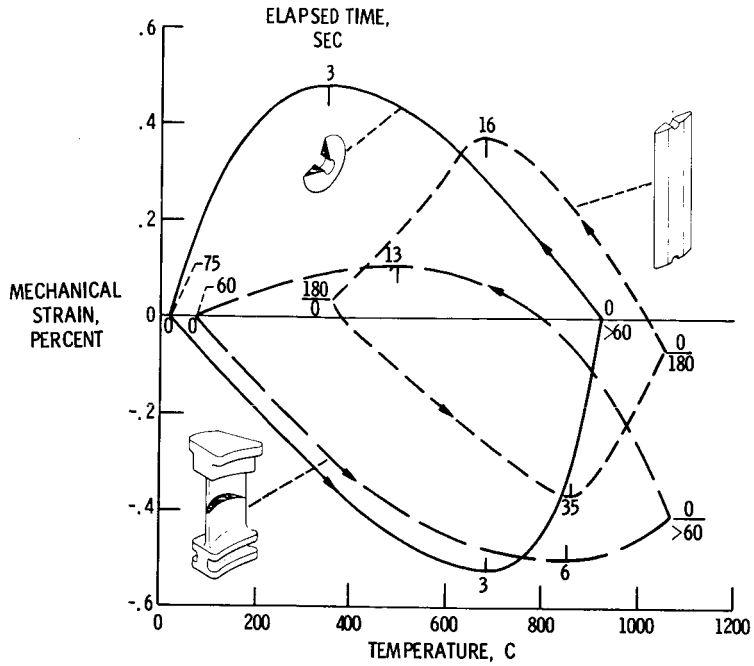

Figure 1. - Typical strain-temperature-time calibration curves (alloys: Nimonic 90 tapered disk, MAR M200 double wedge, B1900 airfoil).

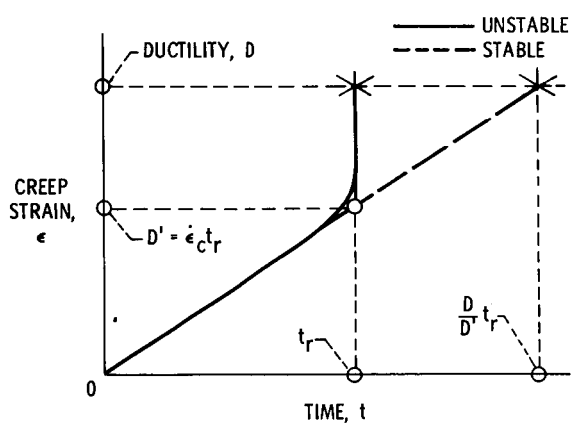

Figure 2. - Idealized creep-rupture behavior.

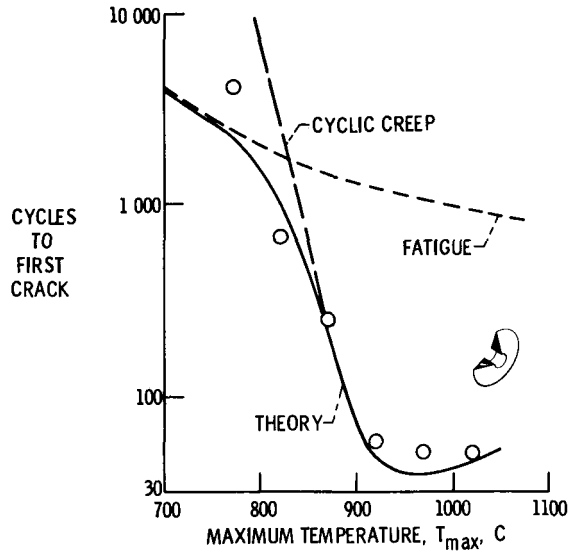

Figure 3. - Comparison of theoretical and experimental thermal fatigue lives of Nimonic 90 tapered disks (0.25 mm edge radius, heating and cooling in fluidized beds, 20 C $\rightleftarrows$ T_{max}, data from ref. 7).

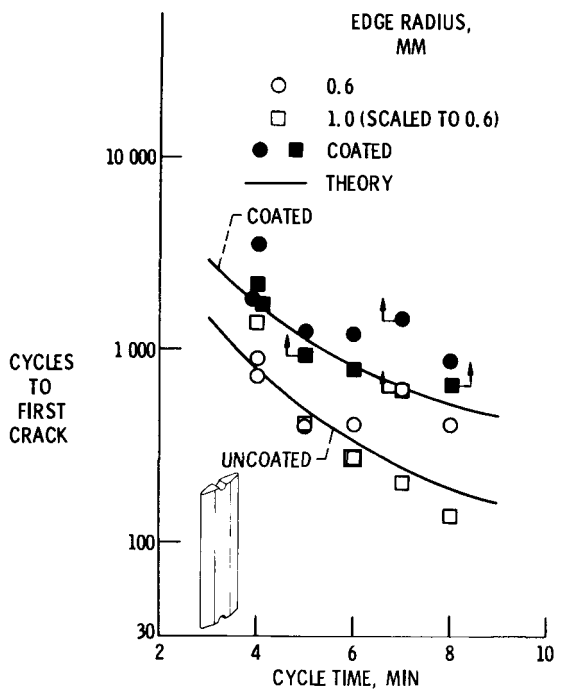

Figure 4. - Comparison of theoretical and experimental thermal fatigue lives of B 1900 double wedges (0.6 and 1.0 mm edge radii, heating and cooling in fluidized beds at 320 and 1090 C, data from refs. 8 and 9).

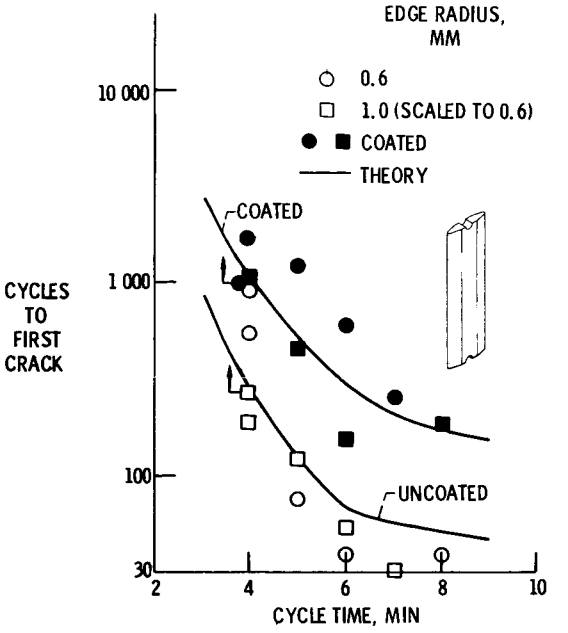

Figure 5. - Comparison of theoretical and experimental thermal fatigue lives of IN 100 double wedges (0.6 and 1.0 mm edge radii, heating and cooling in fluidized beds at 320 and 1090 C, data from refs. 8 and 9).

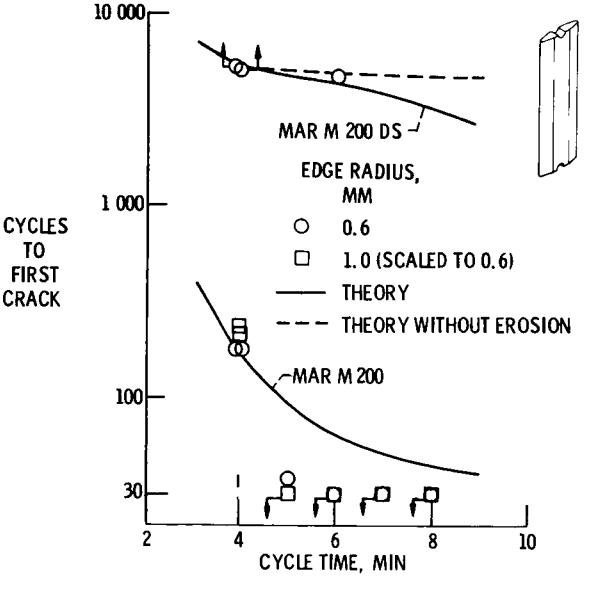

Figure 6. - Comparison of theoretical and experimental thermal fatigue lives of MAR M 200 and MAR M 200 DS double wedges (0.6 and 1.0 mm edge radii, heating and cooling in fluidized beds at 320 and 1090 C, data from refs. 8 and 9).

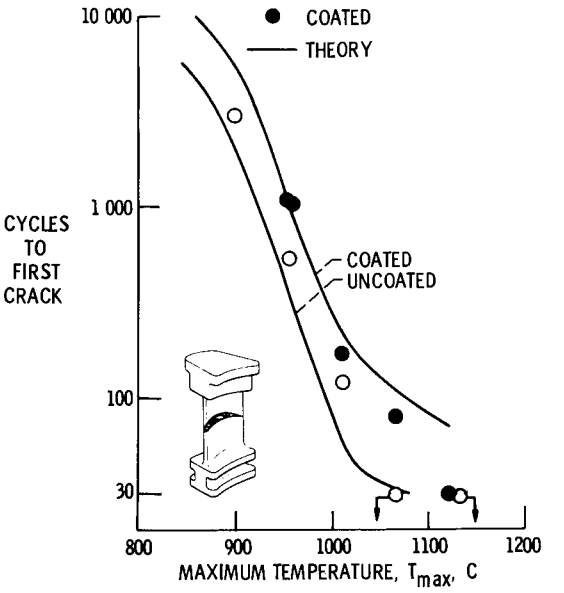

Figure 7. - Comparison of theoretical and experimental thermal fatigue lives of IN 100 cambered airfoils (1.2 mm leading edge radius, heating in Mach 1 burner, rapid air cooling, 75 C $\rightleftarrows T_{max}$, data from ref. 10).

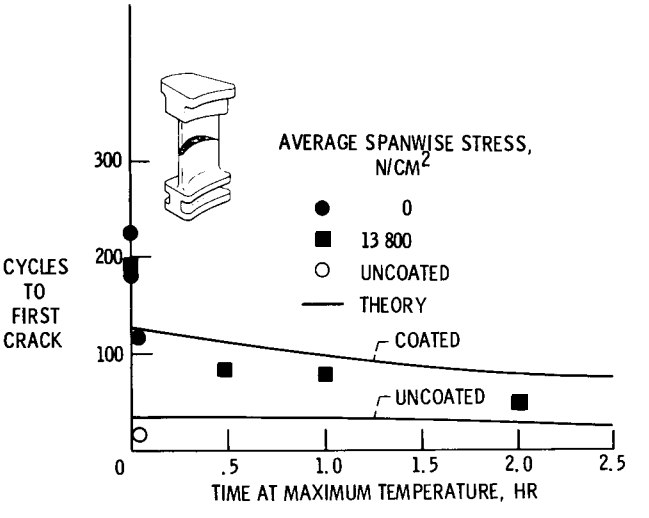

Figure 8. - Comparison of theoretical and experimental thermal fatigue lives of B 1900 cambered airfoils (1.2 mm leading edge radius, heating in Mach 1 burner, rapid air cooling, 75 C $\rightleftarrows$ 1065 C, data from ref. 10).